STRUCTURAL BIOLOGY COMMUNICATIONS

ISSN 2053-230X

High-resolution structure of a Kazal-type serine protease inhibitor from the dengue vector *Aedes aegypti*

Ricardo J. S. Torquato,[a] Stephen Lu,[a] Nadia Helena Martins,[b] Aparecida S. Tanaka[a]* and Pedro José Barbosa Pereira[c,d]*

[a]Department of Biochemistry, Escola Paulista de Medicina, Universidade Federal de São Paulo (UNIFESP), Rua 3 de Maio 100, 04044-020 São Paulo-SP, Brazil, [b]Laboratório Nacional de Biociências – LNBio, Caixa Postal 6192, 13083-970 Campinas-SP, Brazil, [c]IBMC – Instituto de Biologia Molecular e Celular, Universidade do Porto, Rua Alfredo Allen 208, 4200-135 Porto, Portugal, and [d]Instituto de Investigação e Inovação em Saúde, Universidade do Porto, Rua Alfredo Allen 208, 4200-135 Porto, Portugal. *Correspondence e-mail: tanaka.bioq@epm.br, ppereira@ibmc.up.pt

Received 28 March 2017
Accepted 5 July 2017

Edited by N. Sträter, University of Leipzig, Germany

Keywords: anticoagulants; thrombin; trypsin; salivary glands; protein–protein interactions; Kazal inhibitor; *Aedes aegypti*; Dengue fever; Yellow fever; Zika virus.

PDB reference: Kazal-type serine protease inhibitor from the dengue vector *Aedes aegypti*, 5dae

Supporting information: this article has supporting information at journals.iucr.org/f

Blood-feeding exoparasites are rich sources of protease inhibitors, and the mosquito *Aedes aegypti*, which is a vector of *Dengue virus*, *Yellow fever virus*, *Chikungunya virus* and *Zika virus*, is no exception. AaTI is a single-domain, noncanonical Kazal-type serine proteinase inhibitor from *A. aegypti* that recognizes both digestive trypsin-like serine proteinases and the central protease in blood clotting, thrombin, albeit with an affinity that is three orders of magnitude lower. Here, the 1.4 Å resolution crystal structure of AaTI is reported from extremely tightly packed crystals (~22% solvent content), revealing the structural determinants for the observed inhibitory profile of this molecule.

1. Introduction

Aedes aegypti is a well adapted urban mosquito that is capable of transmitting *Dengue fever virus*, *Yellow fever virus* and *Chikungunya virus* during blood feeding (Gubler, 2002; Vega-Rúa *et al.*, 2014). Recently, *A. aegypti* has also been implicated in the transmission of *Zika virus* (Aliota *et al.*, 2016; Chouin-Carneiro *et al.*, 2016).

In haematophagous animals, proteases and their inhibitors play crucial roles by controlling coagulation (Corral-Rodríguez *et al.*, 2009, 2010), platelet aggregation and vasoconstriction (Ribeiro, 1995) during blood acquisition (Takác *et al.*, 2006) or storage (Araujo *et al.*, 2007; Campos *et al.*, 2002, 2004; Soares *et al.*, 2012). Protease inhibitors are classified according to their primary structure and functional similarity among living organisms (Laskowski & Kato, 1980), and they are currently divided into 79 different families (Rawlings *et al.*, 2016). In invertebrates, the Kazal, Kunitz and serpin inhibitor families contain the largest numbers of members.

Kazal-type inhibitors have characteristic structural features including two or three α-helices and a short three-stranded antiparallel β-sheet (Mühlhahn *et al.*, 1994), six cysteine residues forming three disulfide bonds with 1–5/2–4/3–6 topology, and a canonical binding loop (Bode & Huber, 1992). The Kazal family members can be divided into classical and non-classical inhibitors (Hemmi *et al.*, 2005; Fink *et al.*, 1986), and among the latter it is possible to find single-domain [for example leech-derived tryptase inhibitor (LDTI; Sommerhoff *et al.*, 1994), bdellin B-3 (Fink *et al.*, 1986), *A. aegypti* trypsin inhibitor (AaTI; Watanabe *et al.*, 2010) and agaphelin (Waisberg *et al.*, 2014)] and multi-domain [for example rhodniin (Friedrich *et al.*, 1993) and infestin (Campos *et al.*, 2002)]

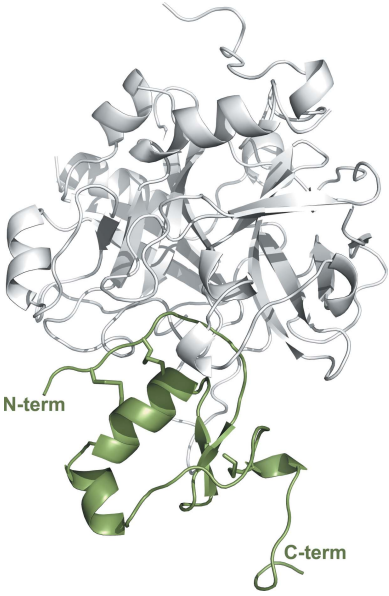

Table 1
Crystallization conditions.

Method	Vapour diffusion, sitting-drop
Plate type	96-well
Temperature (K)	291
Protein concentration (mg ml^{-1})	20
Buffer composition of protein solution	10 m*M* Tris–HCl pH 8.0
Composition of reservoir solution	100 m*M* sodium acetate pH 5.5, 25%(*w*/*v*) PEG 3350, 5%(*v*/*v*) PEG 400, 3%(*v*/*v*) dioxane
Volume and ratio of drop	1 µl (1:1)
Volume of reservoir (µl)	80

proteins. Moreover, the Kazal-type inhibitors present in the midgut of kissing bugs (Triatominae) display strong inhibitory properties against thrombin (Campos *et al.*, 2002; Friedrich *et al.*, 1993; Paim *et al.*, 2011). In the particular case of infestins, a family of multi-domain Kazal-type molecules (Campos *et al.*, 2002), an as yet unknown post-translational processing event generates one or two Kazal-domain inhibitors with distinct specificities from the parent protein (Lovato *et al.*, 2006). Recently, AaTI, a single-domain Kazal-type inhibitor from the mosquito *A. aegypti*, was characterized as a trypsin and thrombin inhibitor (Watanabe *et al.*, 2010). Expression of the gene encoding AaTI was detected in the mosquito salivary gland and midgut, suggesting a role in blood-coagulation control. Interestingly, the enzymatic activity of trypsin-like proteases from the midgut of *A. aegypti* females 24 h post-feeding was strongly inhibited by AaTI, but it only weakly affected enzymatic activity 3 h after feeding (Watanabe *et al.*, 2010). This underscores the specificity of AaTI, since the content of trypsin-like enzymes in the mosquito midgut changes during blood digestion (Noriega & Wells, 1999). In addition, AaTI displays a negatively charged C-terminal sequence, which is reminiscent of that of hirudin (Rydel *et al.*, 1990; Grütter *et al.*, 1990; Fig. 1). Nevertheless, the mechanism of thrombin inhibition by AaTI seems to differ from that of hirudin, since there is no noticeable difference in the inhibition of α-thrombin and γ-thrombin by AaTI, and the removal of the C-terminal tail of the inhibitor does not significantly alter its ability to prolong the thrombin time, suggesting that, in contrast to hirudin, AaTI does not bind to exosite I of thrombin (Watanabe *et al.*, 2011). In the present work, we report the crystallographic three-dimensional structure of AaTI and propose its inhibitory mechanism towards thrombin.

2. Materials and methods

2.1. Macromolecule production

AaTI was expressed in a *Pichia pastoris* system and purified by affinity chromatography on trypsin-Sepharose as described previously (Watanabe *et al.*, 2010).

2.2. Crystallization

The recombinant AaTI sample, concentrated to 20 mg ml^{-1} by ultrafiltration, was used for the screening and optimization of crystallization conditions at Laboratório Robotizado de Cristalização de Proteínas (Robolab-LNLS), Campinas, Brazil. Single crystals were grown at 18°C by sitting-drop vapour diffusion (Table 1). An iodide derivative was prepared by soaking a crystal briefly (∼15 s) in crystallization buffer supplemented with 0.5 *M* NaI. The crystals were directly transferred to the cryostream prior to data collection.

2.3. Data collection and processing

Native (222 images with 1° oscillation and 20 s exposure) and derivative (960 images with 1° oscillation and 20 s exposure) X-ray diffraction data sets were collected from single monoclinic (space group $P2_1$) crystals using a MAR Mosaic 225 CCD detector (marXperts) on beamline MX2 of Laboratório Nacional de Luz Síncrotron (LNLS), Campinas, Brazil (Guimarães *et al.*, 2009). Diffraction data were processed with *XDS* (Kabsch, 2010), scaled with *XSCALE* (Kabsch, 2010) and reduced with utilities from the *CCP*4 suite (Winn *et al.*, 2011; Table 2).

2.4. Structure solution and refinement

The three-dimensional structure of AaTI was solved by SAD using the anomalous signal of iodine with the

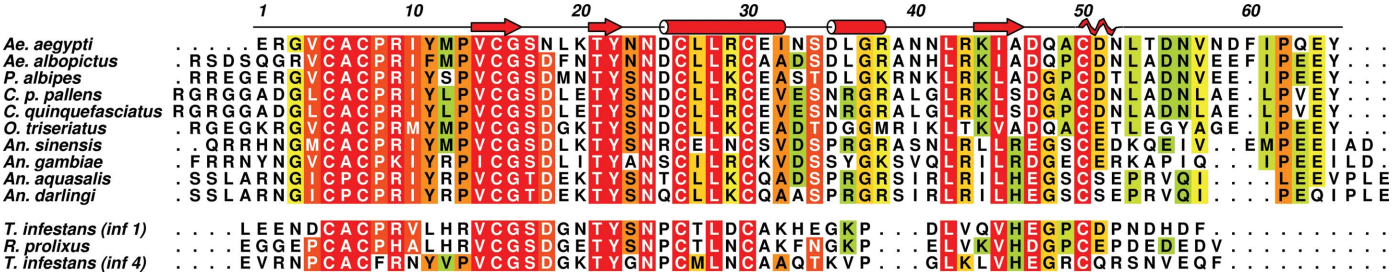

Figure 1
Multiple amino-acid sequence alignment of insect-derived Kazal-type proteins. In the upper block AaTI from *Aedes aegypti* (UniProt entry Q1HRB8) is aligned with other putative Kazal inhibitors from *A. albopictus* (UniProt entry Q5MIW1), *Psorophora albipes* (UniProt entry T1D5N9), *Culex pipiens pallens* (UniProt entry I6XC79), *C. quinquefasciatus* (UniProt entry B0XEZ9), *Ochlerotatus triseriatus* (UniProt entry C6ZQX9), *Anopheles sinensis* (UniProt entry A0A084VPC8), *A. gambiae* (UniProt entry Q7QG67), *A. aquasalis* (UniProt entry T1DGP5) and *A. darlingi* (UniProt entry B6DDZ6). In the lower block, the structurally characterized infestin 1 (PDB entry 2f3c; Campos *et al.*, 2012) and infestin 4 (PDB entry 2erw; Campos *et al.*, 2012) from *Triatoma infestans* and the N-terminal portion of rhodniin (PDB entry 1tbq; van de Locht *et al.*, 1995) from *Rhodnius prolixus* are also aligned with the upper sequences. The mature AaTI amino-acid numbering and secondary-structure elements are indicated above the alignment. A green-to-red colour gradient indicates increasing residue conservation. This figure was prepared with *ALINE* (Bond & Schüttelkopf, 2009).

Table 2
Data collection and processing.

Values in parentheses are for the outer shell.

	Native	Derivative
Diffraction source	W01B-MX2, LNLS	W01B-MX2, LNLS
Wavelength (Å)	1.000	1.459
Temperature (K)	100	100
Detector	MAR Mosaic 225 CCD	MAR Mosaic 225 CCD
Crystal-to-detector distance (mm)	89	99
Rotation range per image (°)	1.0	1.0
Total rotation range (°)	220	960
Exposure time per image (s)	20	20
Space group	$P2_1$	$P2_1$
a, b, c (Å)	26.1, 65.2, 27.7	26.4, 64.0, 27.7
α, β, γ (°)	90, 116.5, 90	90, 117.6, 90
Mosaicity (°)	0.18	0.57
Resolution range (Å)	65.2–1.40 (1.48–1.40)	23.4–1.80 (1.89–1.80)
Total No. of reflections	74704 (10645)	144451 (20019)
No. of unique reflections	16291 (2367)	7491 (1058)
Completeness (%)	99.5 (98.8)	98.0 (94.8)
Multiplicity	4.6 (4.5)	19.3 (18.9)
$\langle I/\sigma(I)\rangle$	11.0 (1.2)	25.7 (6.7)
$R_{\rm r.i.m.}$†	0.080 (1.583)	0.075 (0.371)
$R_{\rm p.i.m.}$‡	0.037 (0.734)	0.017 (0.084)
Half-set correlation $CC_{1/2}$	0.998 (0.568)	1.000 (0.985)
Anomalous half-set correlation $CC_{\rm anom}$		0.853 (0.235)
Overall B factor from Wilson plot (Å^2)	18.3	22.6

† $R_{\rm r.i.m.} = \sum_{hkl}\{N(hkl)/[N(hkl)-1]\}^{1/2}\sum_i |I_i(hkl) - \langle I(hkl)\rangle|/\sum_{hkl}\sum_i I_i(hkl)$.
‡ $R_{\rm p.i.m.} = \sum_{hkl}\{1/[N(hkl)-1]\}^{1/2}\sum_i |I_i(hkl) - \langle I(hkl)\rangle|/\sum_{hkl}\sum_i I_i(hkl)$.

Table 3
Structure solution and refinement.

Values in parentheses are for the outer shell.

Structure solution	
SHELXD	
No. of heavy atoms	3
SHELXE	
FOM	0.570
No. of residues built	88
Refinement	
Resolution range (Å)	32.6–1.40 (1.49–1.40)
Completeness (%)	99.3
σ Cutoff	$F > 1.35\sigma(F)$
No. of reflections, working set	16260 (2549)
No. of reflections, test set	840 (142)
Final $R_{\rm cryst}$	0.180 (0.320)
Final $R_{\rm free}$	0.230 (0.363)
Cruickshank DPI	0.0838
No. of non-H atoms	
Protein	838
Water	89
Total	927
R.m.s. deviations	
Bonds (Å)	0.011
Angles (°)	1.405
Average B factors (Å^2)	
Protein	28.2
Water	33.9
Ramachandran plot	
Most favoured (%)	91.8
Allowed (%)	8.2

SHELXC/*D*/*E* pipeline (Sheldrick, 2010) and the *HKL2MAP* GUI (Pape & Schneider, 2004). An initial atomic model was built with *ARP*/*wARP* (Langer *et al.*, 2008) and was completed manually with *Coot* (Emsley *et al.*, 2010), alternating with cycles of refinement with *PHENIX* (Adams *et al.*, 2010; Table 3). The refined model coordinates and structure factors were deposited in the Protein Data Bank with accession code 5dae.

3. Results and discussion

3.1. Crystallization, data collection and structure solution

Recombinant AaTI crystallized readily at 18°C using a vapour-diffusion technique with a mixture of PEG 3350 and PEG 400 as precipitant, yielding monoclinic crystals that belonged to space group $P2_1$ (Table 1). Native AaTI crystals diffracted to 1.4 Å resolution (Table 2) at a synchrotron source, but initial attempts at structure determination using molecular-replacement techniques with the coordinates of a leech-derived tryptase inhibitor (PDB entry 1ldt; Stubbs *et al.*, 1997), assuming that a single full-length AaTI molecule was present in the asymmetric unit (57.3% solvent content), as suggested by the probability distribution of the Matthews coefficient, failed. Therefore, the native crystals were soaked briefly in crystallization buffer containing sodium iodide and a complete, redundant data set to 1.8 Å resolution was collected using 8.5 keV synchrotron radiation (Table 2). Although maximization of the anomalous signal could have been achieved using a longer wavelength, which was within the reach of the experimental setup, at 8.5 keV a good compromise was found between anomalous signal and photon flux. The structure was solved by single-wavelength anomalous dispersion using the anomalous signal of iodide, and the experimental maps revealed the presence of two inhibitor molecules in the asymmetric unit. The molecular mass of the full-length inhibitor (7.4 kDa) and the small unit-cell volume (∼42 000 Å^3) would result in an extremely low (<15%) solvent content for these samples. However, we observed unwanted processing of AaTI during heterologous expression, and the recombinant material contained a mixture of full-length AaTI and several truncated forms (data not shown). Mass-spectrometric analysis of the AaTI crystals identified an AaTI fragment spanning residues Glu1–Asp59, which is in good agreement with the segments that could be modelled in the electron-density maps: residues Gly3–Asp59 for AaTI molecule *A* and Arg2–Thr54 for molecule *B*. Considering the presence of this truncated form of AaTI in the asymmetric unit, the crystals displayed an unusually low solvent content of ∼22–23% and consequently tight crystal packing (Fig. 2; Offermann *et al.*, 2015; Trillo-Muyo *et al.*, 2013). The unusually tight packing of the AaTI crystals led to an erroneous initial assessment of the asymmetric unit composition, explaining why the attempts at phasing using molecular replacement failed. One of the three iodide ions that could be located (Table 3) is in the vicinity of molecule *A* (close to Tyr22 and Asn23), another is closer to molecule *B* (Lys44) and the third is at the interface between both molecules, close to the side chains of Ile10 and Cys26 of molecule *A* and of Met12 of molecule *B*.

3.2. Overall structure

AaTI displays a typical Kazal-domain structure, with central α-helical segments spanning residues 25–32 and 35–38 that, together with a short C-terminal 3_{10}-helix, border the small central three-stranded antiparallel β-sheet (Figs. 1 and 3). With only one amino acid separating the two first cysteine residues, AaTI can be unambiguously placed in the group of nonclassical Kazal-domain inhibitors (Fink *et al.*, 1986), displaying highest sequence identity to other mosquito Kazal-domain proteins (Fig. 1). From a structural point of view, AaTI is most similar to three other insect Kazal inhibitors: infestins 1 and 4 from *Triatoma infestans* and rhodniin from *Rhodnius prolixus* (Campos *et al.*, 2012; van de Locht *et al.*, 1995; Fig. 3). The conservation of an arginine residue (Arg8; Fig. 1) at position P1 of the putative reactive loop of AaTI is also noteworthy, reinforcing its observed preference for trypsin-like proteinases (Watanabe *et al.*, 2010).

Unsurprisingly, the two AaTI molecules in the asymmetric unit are very similar, with an r.m.s.d. of 0.61 Å for 48 aligned C^{α} atoms (Fig. 3). Indeed, all observable differences can be attributed to intrinsic flexibility (for example the N- and C-terminal regions) or crystal-packing effects. The electron-density maps are of very good quality, with all built residues defined, except for the distal portions (past the C^{γ} atom) of a few side chains (for example Leu36, Asn41 and Asn58 of molecule *A*). Since the flexible C-terminal region is more ordered in AaTI molecule *A*, it was used for all comparisons with other Kazal-inhibitors described below.

3.3. Inhibition specificity

Although AaTI does not inhibit the trypsin-like serine proteinases human plasma kallikrein or coagulation factors Xa and XIIa (Watanabe *et al.*, 2010), it behaves as a competitive inhibitor of plasmin (K_i = 3.8 n*M*; Watanabe *et al.*, 2010) and bovine trypsin (K_i = 0.15 n*M*; Watanabe *et al.*, 2010), with a potency comparable to that of infestin 1–2 (K_i = 3.1 n*M*; Campos *et al.*, 2004). Superposition of the three-dimensional model of AaTI with that of infestin 1 in complex with bovine trypsin (PDB entry 2f3c; Campos *et al.*, 2012) highlights the full conservation of the enzyme–inhibitor contacts, which is in perfect agreement with the observed inhibitory activity of AaTI towards trypsin. In contrast, although AaTI displays anticoagulant activity in the form of prolongation of the prothrombin time, activated partial thromboplastin time and thrombin time (Watanabe *et al.*, 2010), its affinity for thrombin (K_i = 320 n*M*; Watanabe *et al.*, 2011) is four orders of magnitude lower than that of infestin 1–2 (K_i = 0.025 n*M*; Campos *et al.*, 2004). Indeed, superposition of the AaTI model on the N-terminal domain of rhodniin in complex with thrombin (PDB entry 1tbq; van de Locht *et al.*, 1995) reveals

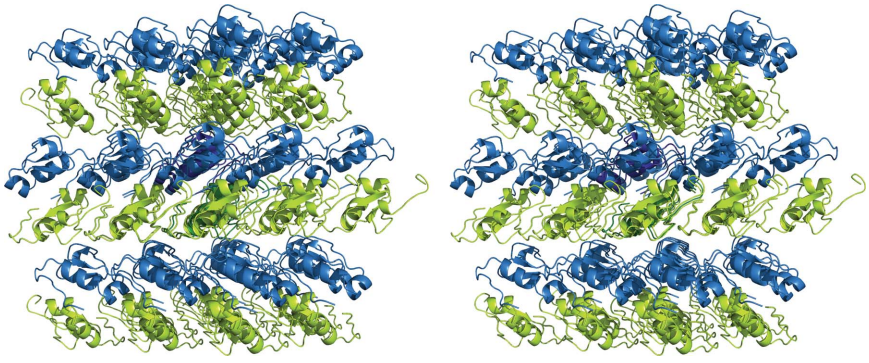

Figure 2
Stereoscopic view of the AaTI crystal packing. The two AaTI monomers in the asymmetric unit (molecule *A* in blue, molecule *B* in green) are displayed in ribbon representation, together with surrounding symmetry mates, highlighting the tight packing of the crystals. This figure was prepared with *PyMOL* (http://www.pymol.org).

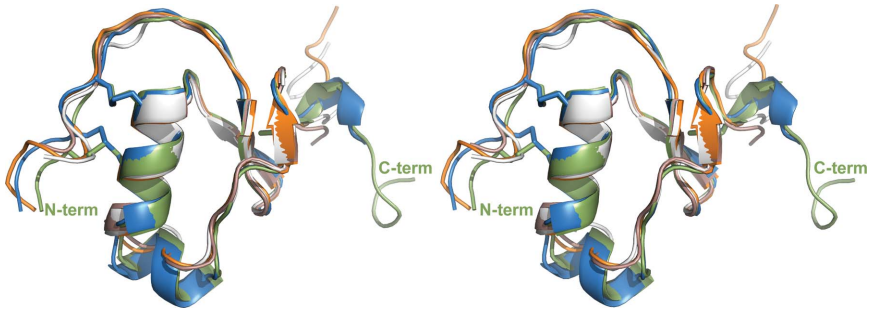

Figure 3
Structural alignment of AaTI monomers with other Kazal-type inhibitors. The two AaTI molecules (molecule *A* in green, molecule *B* in blue) in the asymmetric unit were superposed using *LSQMAN* (Kleywegt, 1996). The N- and C-termini of molecule *A* are labelled. The AaTI monomers are superposed on the closest structural homologues, as identified by the *DALI* server (Holm & Rosenström, 2010): infestin 1 (pink; PDB entry 2f3c; Campos *et al.*, 2012), infestin 4 (white; PDB entry 2erw; Campos *et al.*, 2012) and the N-terminal domain of rhodniin (orange; PDB entry 1tbq; van de Locht *et al.*, 1995). This figure was prepared with *PyMOL* (http://www.pymol.org).

significant structural differences between the two Kazal domains that would result in important steric clashes between AaTI and the 60-loop of thrombin: Ala11 and Pro26 in rhodniin are replaced by the bulkier Ile10 and Asp25, respectively (Fig. 1). The side chains of both residues would clash significantly with that of Trp60D from the 60-loop of thrombin, impacting binding (Figs. 4*a* and 4*b*), which is in line with the observed lower affinity of AaTI towards thrombin. In contrast, in the thrombin-inhibiting infestin 1 a single noteworthy replacement is observed, with a slightly larger valine residue occupying the position equivalent to Ala11 in rhodniin. Further, there are two other nonconservative replacements in AaTI that could impact its affinity towards thrombin: Asn23 and Leu27, which replace Ser24 and Thr28, respectively, of both rhodniin and infestin 1 (Fig. 1). The former would require a readjustment of the positions of Trp148 and Asn143 from the protease, while the latter would not only clash with Glu192 from thrombin, but the observed polar interaction with this residue would also not be established (Fig. 4*c*). The steric clashes of AaTI with the active-site region of thrombin resemble those identified for LDTI, in which the replacement of bulky residues potentially colliding with the protuberant 60-loop of the proteinase, including Ile9 and Ser24 (Ile10 and Asp25 in AaTI), increased the affinity for thrombin by several orders of magnitude (Morenweiser *et al.*, 1997).

In the conformation that is observed in these crystals, the C-terminal tail of AaTI would point away from the proteinase–inhibitor interaction surface upon canonical binding to thrombin. However, given its flexible nature, it is conceivable that the C-terminal segment of AaTI could extend along the surface of the proteinase, reaching the proximal region of exosite I. This hypothesis lacks experimental support, since it has previously been shown that AaTI inhibits α-thrombin and exosite I-disrupted γ-thrombin with similar efficiency (Watanabe *et al.*, 2011), in contrast to what is observed for other exosite I-targeting inhibitors (for example hirudin), which display a much decreased inhibition potency towards γ-thrombin (Ascenzi *et al.*, 1992). In agreement with this, in the bidentate binding of rhodniin to thrombin a significant contribution towards the observed affinity is attributable to

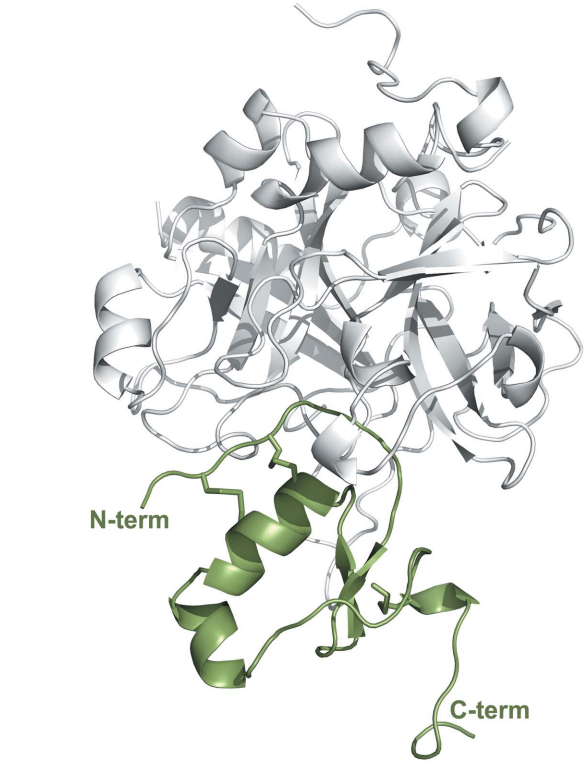

(*a*)

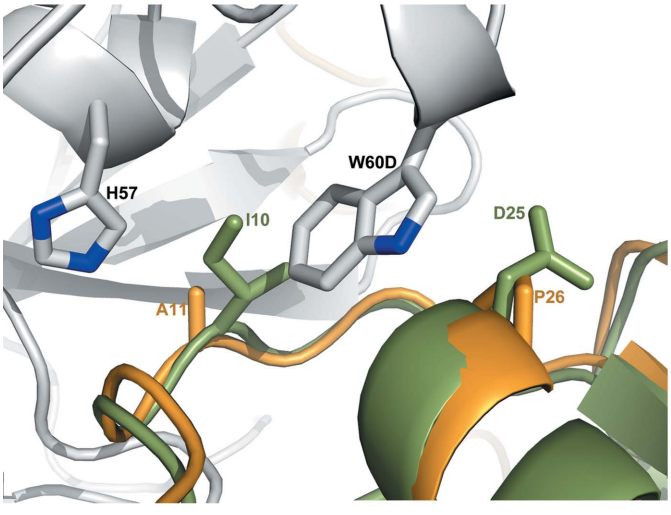

(*b*)

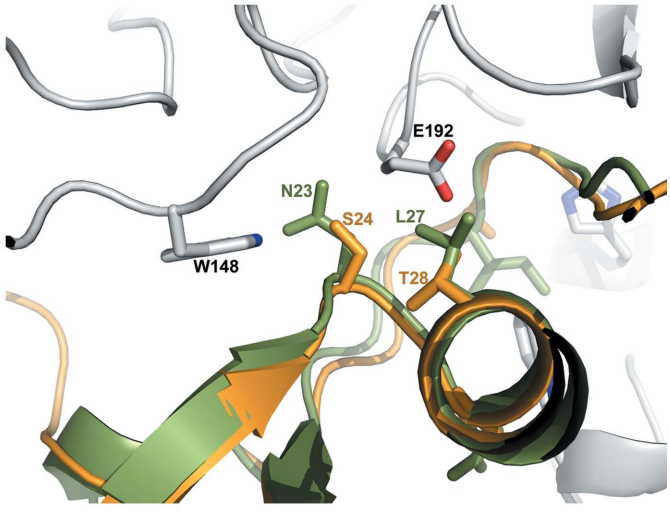

(*c*)

Figure 4
Details of the interaction between AaTI and thrombin. (*a*) AaTI (green) was docked into the active site of thrombin (grey) by superposing it on the N-terminal domain of thrombin-bound rhodniin (PDB entry 1tbq; van de Locht *et al.*, 1995). The N- and C-termini of AaTI are labelled. (*b*) Close-up of the interactions between AaTI and the 60-loop of thrombin, with a superposed rhodniin N-terminal domain [AaTI and thrombin colours as in (*a*); rhodniin is shown as an orange ribbon]. Relevant side chains are represented as sticks and labelled. (*c*) Close-up of the interactions between AaTI and Glu192 and the autolysis loop of thrombin, with a superposed rhodniin N-terminal domain [colours as in (*b*)]. Relevant side chains are represented as sticks and labelled. This figure was prepared with *PyMOL* (http://www.pymol.org).

the interactions established by the C-terminal, exosite I-targeting domain of the inhibitor (van de Locht *et al.*, 1995). The considerable level of sequence identity between infestin 1–2 and rhodniin suggests that the mechanism of binding to thrombin is also conserved in the two inhibitors (Campos *et al.*, 2002). It is worth noting that grafting the acidic C-terminal region of hirudin onto LDTI converts it into an efficient thrombin inhibitor (Morenweiser *et al.*, 1997), an effect that is cumulative with the mutation of bulky amino acids within the reactive–site loop. Together, these changes convert LDTI from a mediocre (K_i > 300 n*M*) to a very good (K_i = 16.0 p*M*) thrombin inhibitor.

On the other hand, this seemingly plausible canonical binding of AaTI to thrombin does not support an interaction between the C-terminal region of the inhibitor and exosite II of thrombin, as observed for haemadin (Richardson *et al.*, 2000). Considering that the structural features of the reactive loop and the surrounding regions of AaTI can satisfactorily explain its relatively low affinity for thrombin, canonical binding to the proteinase is indeed the most plausible mechanism for thrombin inhibition by AaTI. This is further underscored by the observed mild effect of disruption of thrombin exosite I in inhibition by AaTI, as well as by the significant anticlotting activity of C-terminally truncated AaTI, as measured by a thrombin-time assay (Watanabe *et al.*, 2011). The seemingly minor contribution of the C-terminal acidic tail of AaTI to the interaction with thrombin does not explain the presence of a similar segment in related inhibitors from other species (Fig. 1), and therefore a different physiological (and hitherto unidentified) role cannot be ruled out because this segment alone displayed an observable effect in the prolongation of the clotting time of plasma (Watanabe *et al.*, 2011).

Acknowledgements

This work was supported by the Brazilian Synchrotron Light Laboratory (LNLS). We thank Dr Alexandre Tashima (Department of Biochemistry, Universidade Federal de São Paulo, Brazil) for mass-spectrometric analyses.

Funding information

This work was supported by research grants from FAPESP (12/03657-8) and from CNPq (478504/2013-6, 400835/2014-2 and 308780/2013-2). PJBP also acknowledges the financial support received through the Special Visiting Researcher Program (PVE – Bolsa Pesquisador Visitante Especial) with reference 400835/2014-2. This work was funded in part by Portuguese funds through FCT – Fundação para a Ciência e a Tecnologia in the form of the 'Institute for Research and Innovation in Health Sciences' project (POCI-01-0145-FEDER-007274), co-funded by the European Regional Development Fund (FEDER) through the COMPETE 2020 – Operational Programme for Competitiveness and Internationalization (POCI), PORTUGAL 2020. Support from the 'Structured program on bioengineered therapies for infectious diseases and tissue regeneration' (Norte-01-0145-FEDER-000012), funded by the Norte Portugal Regional Operational Programme (NORTE 2020) under the PORTUGAL 2020 Partnership Agreement through FEDER, is also acknowledged. AST is a research fellow of the CNPq.

References

Adams, P. D. *et al.* (2010). *Acta Cryst.* D**66**, 213–221.
Aliota, M. T., Peinado, S. A., Velez, I. D. & Osorio, J. E. (2016). *Sci. Rep.* **6**, 28792.
Araujo, R. N., Campos, I. T., Tanaka, A. S., Santos, A., Gontijo, N. F., Lehane, M. J. & Pereira, M. H. (2007). *Int. J. Parasitol.* **37**, 1351–1358.
Ascenzi, P., Amiconi, G., Coletta, M., Lupidi, G., Menegatti, E., Onesti, S. & Bolognesi, M. (1992). *J. Mol. Biol.* **225**, 177–184.
Bode, W. & Huber, R. (1992). *Eur. J. Biochem.* **204**, 433–451.
Bond, C. S. & Schüttelkopf, A. W. (2009). *Acta Cryst.* D**65**, 510–512.
Campos, I. T. N., Amino, R., Sampaio, C. A. M., Auerswald, E. A., Friedrich, T., Lemaire, H.-G., Schenkman, S. & Tanaka, A. S. (2002). *Insect Biochem. Mol. Biol.* **32**, 991–997.
Campos, I. T. N., Souza, T. A. C. B., Torquato, R. J. S., De Marco, R., Tanaka-Azevedo, A. M., Tanaka, A. S. & Barbosa, J. A. R. G. (2012). *Acta Cryst.* D**68**, 695–702.
Campos, I. T. N., Tanaka-Azevedo, A. M. & Tanaka, A. S. (2004). *FEBS Lett.* **577**, 512–516.
Chouin-Carneiro, T., Vega-Rua, A., Vazeille, M., Yebakima, A., Girod, R., Goindin, D., Dupont-Rouzeyrol, M., Lourenço-de-Oliveira, R. & Failloux, A. B. (2016). *PLoS Negl. Trop. Dis.* **10**, e0004543.
Corral-Rodríguez, M. A., Macedo-Ribeiro, S., Pereira, P. J. B. & Fuentes-Prior, P. (2009). *Insect Biochem. Mol. Biol.* **39**, 579–595.
Corral-Rodríguez, M. A., Macedo-Ribeiro, S., Pereira, P. J. B. & Fuentes-Prior, P. (2010). *J. Med. Chem.* **53**, 3847–3861.
Emsley, P., Lohkamp, B., Scott, W. G. & Cowtan, K. (2010). *Acta Cryst.* D**66**, 486–501.
Fink, E., Rehm, H., Gippner, C., Bode, W., Eulitz, M., Machleidt, W. & Fritz, H. (1986). *Biol. Chem. Hoppe Seyler*, **367**, 1235–1242.
Friedrich, T., Kröger, B., Bialojan, S., Lemaire, H. G., Höffken, H. W., Reuschenbach, P., Otte, M. & Dodt, J. (1993). *J. Biol. Chem.* **268**, 16216–16222.
Grütter, M. G., Priestle, J. P., Rahuel, J., Grossenbacher, H., Bode, W., Hofsteenge, J. & Stone, S. R. (1990). *EMBO J.* **9**, 2361–2365.
Gubler, D. J. (2002). *Trends Microbiol.* **10**, 100–103.
Guimarães, B. G., Sanfelici, L., Neuenschwander, R. T., Rodrigues, F., Grizolli, W. C., Raulik, M. A., Piton, J. R., Meyer, B. C., Nascimento, A. S. & Polikarpov, I. (2009). *J. Synchrotron Rad.* **16**, 69–75.
Hemmi, H., Kumazaki, T., Yoshizawa-Kumagaye, K., Nishiuchi, Y., Yoshida, T., Ohkubo, T. & Kobayashi, Y. (2005). *Biochemistry*, **44**, 9626–9636.
Holm, L. & Rosenström, P. (2010). *Nucleic Acids Res.* **38**, W545–W549.
Kabsch, W. (2010). *Acta Cryst.* D**66**, 125–132.
Kleywegt, G. J. (1996). *Acta Cryst.* D**52**, 842–857.
Langer, G., Cohen, S. X., Lamzin, V. S. & Perrakis, A. (2008). *Nature Protoc.* **3**, 1171–1179.
Laskowski, M. Jr & Kato, I. (1980). *Annu. Rev. Biochem.* **49**, 593–626.
Locht, A. van de, Lamba, D., Bauer, M., Huber, R., Friedrich, T., Kröger, B., Höffken, W. & Bode, W. (1995). *EMBO J.* **14**, 5149–5157.
Lovato, D. V., Nicolau de Campos, I. T., Amino, R. & Tanaka, A. S. (2006). *Biochimie*, **88**, 673–681.
Morenweiser, R., Auerswald, E. A., van de Locht, A., Fritz, H., Stürzebecher, J. & Stubbs, M. T. (1997). *J. Biol. Chem.* **272**, 19938–19942.

Mühlhahn, P., Czisch, M., Morenweiser, R., Habermann, B., Engh, R. A., Sommerhoff, C. P., Auerswald, E. A. & Holak, T. A. (1994). *FEBS Lett.* **355**, 290–296.
Noriega, F. G. & Wells, M. A. (1999). *J. Insect Physiol.* **45**, 613–620.
Offermann, L. R., Bublin, M., Perdue, M. L., Pfeifer, S., Dubiela, P., Borowski, T., Chruszcz, M. & Hoffmann-Sommergruber, K. (2015). *J. Agric. Food Chem.* **63**, 9150–9158.
Paim, R. M. M., Araújo, R. N., Soares, A. C., Lemos, L. C., Tanaka, A. S., Gontijo, N. F., Lehane, M. J. & Pereira, M. H. (2011). *Int. J. Parasitol.* **41**, 765–773.
Pape, T. & Schneider, T. R. (2004). *J. Appl. Cryst.* **37**, 843–844.
Rawlings, N. D., Barrett, A. J. & Finn, R. (2016). *Nucleic Acids Res.* **44**, D343–D350.
Ribeiro, J. M. (1995). *Infect. Agents Dis.* **4**, 143–152.
Richardson, J. L., Kröger, B., Hoeffken, W., Sadler, J. E., Pereira, P., Huber, R., Bode, W. & Fuentes-Prior, P. (2000). *EMBO J.* **19**, 5650–5660.
Rydel, T. J., Ravichandran, K. G., Tulinsky, A., Bode, W., Huber, R., Roitsch, C. & Fenton, J. W. II (1990). *Science*, **249**, 277–280.
Sheldrick, G. M. (2010). *Acta Cryst.* D**66**, 479–485.
Soares, T. S., Watanabe, R. M., Tanaka-Azevedo, A. M., Torquato, R. J., Lu, S., Figueiredo, A. C., Pereira, P. J. & Tanaka, A. S. (2012). *Vet. Parasitol.* **187**, 521–528.
Sommerhoff, C. P., Söllner, C., Mentele, R., Piechottka, G. P., Auerswald, E. A. & Fritz, H. (1994). *Biol. Chem. Hoppe Seyler*, **375**, 685–694.
Stubbs, M. T., Morenweiser, R., Stürzebecher, J., Bauer, M., Bode, W., Huber, R., Piechottka, G. P., Matschiner, G., Sommerhoff, C. P., Fritz, H. & Auerswald, E. A. (1997). *J. Biol. Chem.* **272**, 19931–19937.
Takác, P., Nunn, M. A., Mészáros, J., Pechánová, O., Vrbjar, N., Vlasáková, P., Kozánek, M., Kazimírová, M., Hart, G., Nuttall, P. A. & Labuda, M. (2006). *J. Exp. Biol.* **209**, 343–352.
Trillo-Muyo, S., Jasilionis, A., Domagalski, M. J., Chruszcz, M., Minor, W., Kuisiene, N., Arolas, J. L., Solà, M. & Gomis-Rüth, F. X. (2013). *Acta Cryst.* D**69**, 464–470.
Vega-Rúa, A., Zouache, K., Girod, R., Failloux, A. B. & Lourenço-de-Oliveira, R. (2014). *J. Virol.* **88**, 6294–6306.
Waisberg, M. *et al.* (2014). *PLoS Pathog.* **10**, e1004338.
Watanabe, R. M., Soares, T. S., Morais-Zani, K., Tanaka-Azevedo, A. M., Maciel, C., Capurro, M. L., Torquato, R. J. & Tanaka, A. S. (2010). *Biochimie*, **92**, 933–939.
Watanabe, R. M., Tanaka-Azevedo, A. M., Araujo, M. S., Juliano, M. A. & Tanaka, A. S. (2011). *Biochimie*, **93**, 618–623.
Winn, M. D. *et al.* (2011). *Acta Cryst.* D**67**, 235–242.